ARTICLE

pubs.acs.org/Biomac

Levan Nanostructured Thin Films by MAPLE Assembling

Felix Sima,[†] Esra Cansever Mutlu,[‡] Mehmet S. Eroglu,[§,∥] Livia E. Sima,[⊥] Natalia Serban,[†] Carmen Ristoscu,[†] Stefana M. Petrescu,[⊥] Ebru Toksoy Oner,[‡] and Ion N. Mihailescu*[,†]

[†]Lasers Department, National Institute for Lasers, Plasma and Radiation Physics, 409 Atomistilor Street, Magurele, Ilfov, RO-77125, Romania

[‡]Department of Bioengineering and [§]Department of Chemical Engineering, Marmara University, Goztepe 34722 Istanbul, Turkey

[∥]TUBITAK-UME, Chemistry Group Laboratories, PO Box 54, 41471 Gebze, Kocaeli, Turkey

[⊥]Institute of Biochemistry of Romanian Academy, Splaiul Independentei 296, Bucharest, Romania

ABSTRACT: Synthesis of nanostructured thin films of pure and oxidized levan exopolysaccharide by matrix-assisted pulsed laser evaporation is reported. Solutions of pure exopolysaccharides in dimethyl sulfoxide were frozen in liquid nitrogen to obtain solid cryogenic pellets that have been used as targets in pulsed laser evaporation experiments with a KrF* excimer source. The expulsed material was collected and assembled onto glass slides and Si wafers. The contact angle studies evidenced a higher hydrophilic behavior in the case of oxidized levan structures because of the presence of acidic aldehyde−hydrogen bonds of the coating formed after oxidation. The obtained films preserved the base material composition as confirmed by Fourier transform infrared spectroscopy. They were compact with high specific surface areas, as demonstrated by scanning electron and atomic force microscopy investigations. In vitro colorimetric assays revealed a high potential for cell proliferation for all coatings with certain predominance for oxidized levan.

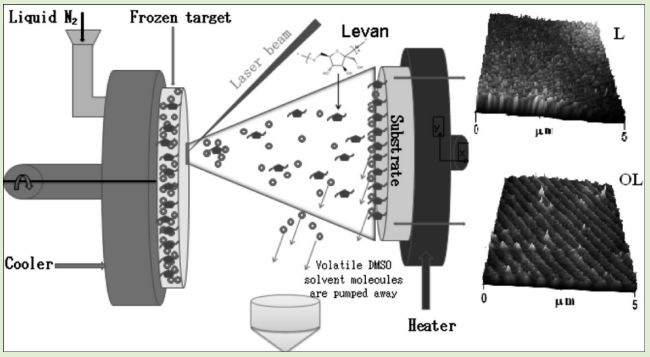

INTRODUCTION

Exopolysaccharides (EPSs) are high-molecular-weight polymers that are composed of sugar residues and are secreted by microorganisms in the surrounding environment to serve as a protective barrier against external stress. They are good candidates for many prospective applications because of their unique physicochemical and rheological properties, biocompatibility, and biodegradability and have therefore received considerable interest in recent years.[1] Unlike mesophilic producers of EPSs, which are mostly pathogenic, extremophilic microorganisms provide nonpathogenic products, suitable for applications in food industry, pharmacy, and cosmetics as emulsifiers, stabilizers, gel agents, coagulants, thickeners, and suspending agents.[2] One extremophilic EPS producer is the halophilic *Halomonas* sp. AAD6 strain yielding high levels of levan, which is a long linear homopolymer of $\beta(2-6)$-linked fructose residues.[3] As a water-soluble, strongly adhesive and film-forming biopolymer, levan is distinguished from other polysaccharides by its valuable properties like low viscosity, high solubility in oil, compatibility with salts and surfactants, stability to heat, acid, and alkali media, high holding capacity for water and chemicals, and good biocompatibility. Hence, levan has many potential uses as emulsifier, stabilizer and thickener, encapsulating agent, osmoregulator, and cryoprotector in food, cosmetics, pharmaceutical, or chemical industries. In medicine, levan is used as plasma substitute, prolongator of drug activity, radio protector, antitumor, and antihyperlipidemic agent.[4] Levan by *Halomonas* sp. has recently been reported as a good candidate for development of nanocarrier systems for peptide and protein drug delivery.[5] Considerable decrease in the fabrication expenses of this polymer has been reported by optimization of fermentation conditions in large-scale levan production by *Halomonas* sp. bioreactor cultures.[6]

Likewise, levan coatings could have great commercial potential for specific applications. Currently, films of polymers with desired shape and area are obtained by solvent casting[7] or thermal processing.[8] Presently, drug tablet coatings consist of polymer and polysaccharide, with plasticizers and pigments included. By extrusion and molding, hundreds of micrometers thick films of levan were prepared by adding glycerol as a plasticizer.[9] However, as known, the thicker the film, the higher the risks of poor adhesion, cracking, or easy peeling[10] and thus the harder to control the film dissolution.

Films on the nanometric scale would reduce the cost of production and increase the specific surface area. For drug release and delivery, thin coatings of desired thickness would be attractive to control the rate of dissolution in the gastrointestinal tract because some drugs are absorbed better at different points in the digestive system. Nanostructured layers could boost the potential

Received: March 13, 2011
Revised: April 26, 2011
Published: April 26, 2011

of the biopolymer surface for applications as nanocarriers or drug delivery. Moreover, uniform distribution on different collectors allows for a wide range of new uses, especially in biology and medicine.

Matrix-assisted pulsed laser evaporation (MAPLE) was developed for the controlled growth of biopolymer thin films.[11] In MAPLE, the laser-induced material ejection is generated backward from solid cryogenic targets, and the expulsed substance is assembled on specific collectors. Typically, the targets consist of the organic complex dissolved into a laser wavelength absorbing solvent when frozen. At rather low laser fluences, the thermal and chemical decomposition are minimal and the safe transfer of the organic compound is ensured. The method permitted the fabrication of micro- or nanoarrays of wide-ranging biomaterials[12,13] with applications in optoelectronics,[14] biosensing,[15] chemical sensing, and [16] biochemical analysis as well as for drug delivery systems[17] and implant development.[18]

For the first time with the present study, MAPLE was extended to obtain nanostructured thin films of levan (L) and oxidized levan (OL) under vacuum conditions. The films were characterized physicochemically, and the biocompatible behavior was investigated. The morphological features, compositional characteristics, and biological functions were described, and possible correlations were analyzed.

MATERIALS AND METHODS

Growth Conditions and Purification of Levan. Bacterial strain *Halomonas* sp. AAD6 (JCM15723, DSM 21644, GenBank accession number DQ131909) was cultivated under controlled bioreactor conditions using a semichemical medium with the following composition in $g \cdot L^{-1}$: 137.2 NaCl; 50 sucrose; 7 K_2HPO_4; 2 KH_2PO_4; 0.1 $MgSO_4 \cdot 7H_2O$; 1 $(NH_4)_2SO_4$, and 0.5 peptone. The BIOSTAT Q multifermenter of 500 mL working volume was employed. During cultivation, the temperature and pH were kept constant at 37 °C and pH 7. The aeration rate was 0.1 vvm, whereas the agitation was set to 200 rpm. At the stationary phase of growth, cells were precipitated by centrifugation, and levan in the supernatant phase was recovered by ethanol addition, followed by centrifugation. The levan pellet was resuspended in distilled water, dialyzed against distilled water for at least 3 days, and then lyophilized. Levan was further purified by passing through a DEAE-sepharose CL-6B column to remove the impurities. Fractions containing pure levan were collected, tested for total carbohydrate, protein, and nucleic acid contents, and then dried by lyophilization.[3]

Oxidation of Levan. Pure levan samples were subjected to periodate oxidation by prolonged magnetic stirring in a beaker. 0.5 g pure levan was dissolved in 300 mL of distilled water and after the addition of 2 g KIO_4, the solution was stirred at 300 rpm in dark oven at 50 °C for 6 days. After periodate was eliminated from the solution by dialysis against distilled water for at least 48 h, the polymer solution was lyophilized. The formation of aldehyde groups was ascertained by FTIR and quantified by both NMR and by thiosulfate titration.[19]

MAPLE Experiments. For the preparation of the targets used in the deposition process, 0.05 g of L or OL was dissolved in 10 mL of dimethyl sulfoxide (DMSO) to obtain a homogeneous solution. The solution was frozen in liquid N_2 to obtain a solid target that was kept frozen during the deposition process with the aid of a cooler. DMSO was selected as solvent because it does not chemically interact with L or OL and it is volatile and absorbent of 248 nm laser wavelength. As a result, DMSO molecules were vaporized and removed from the reaction chamber by pumping system, whereas levan molecules were transferred to the substrates without degradation.

In the experiments, a KrF* excimer laser source (λ = 248 nm, τ = 25 ns), COMPexPro 205 from Lambda Physik/Coherent radiation was used. The appropriate deposition parameters such as fluence, pulse repetition rate, substrate temperature, and distance between the target and collector were identified after repeated tests. The optimum fluence value changed from 280 $mJ \cdot cm^{-2}$ for L to 350 $mJ \cdot cm^{-2}$ for OL at a pulse repetition rate of 3 Hz. Double-faced polished single-crystalline Si (111) wafers and optical glass slides were ultrasonically cleaned in acetone, ethanol, and deionized water and blown dried with high purity N_2 gas before using as substrates for thin film deposition. The substrates were heated to 100 °C and placed parallel at 3.5 cm separation distance from the rotating frozen target. The dynamic pressure inside the deposition chamber was kept at 5 Pa. For the growth of each L or OL film, 20 000 laser pulses were applied.

Table 1. Surface Free Energy Components of the Liquid Probes ($mJ \cdot m^{-2}$)[21]

liquid	γ_l^{TOT}	γ_l^{LW}	γ_l^{AB}	γ_l^{+}	γ_l^{-}
water	72.8	21.8	51.0	25.5	25.5
formamide	58.0	39.0	19.0	2.28	39.6
glycerol	64.0	34.0	30.0	3.92	57.4
paraffin oil	28.9	28.9	0	0	0

Surface Wettability. The contact angle (CA) measurements were carried out using a Kürüss DSA-100 model CA meter equipped with a single direct dosing system consisting of a high-performance frame grabber camera T1C (25 frames per second) and controlled by a DS3210 software, providing the static and dynamic operation mode. The CA values were determined by sessile drop technique for liquid probes of deionized water, formamide, paraffin oil, and glycerol supplied by Aldrich without supplementary purification. We deposited 5 μL drops of each liquid probe on a dry and clean surface using the autodosing system. Static CAs were measured immediately after the formation of sessile drops of liquid on the surface. Measurements were performed at room temperature and ambient humidity. All reported CA values are averages of three measurements with a standard deviation of $\pm 2°$.[20] Deionized water was used for the determination of acid−base interaction.

The surface free energy and its Liftshitz−van der Waals (LW) and electron-donor and electron-acceptor components (i.e., apolar LW and polar interactions) of the L- and OL-coated samples were calculated by using the following equation, which was mainly based on Young−Dupre theory, which was improved later by van Oss, Good, and Chaudhury.[21−24]

$$\gamma_l(1+\cos\theta) = 2(\gamma_s^{LW}\gamma_l^{LW})^{1/2} + 2(\gamma_s^{+}\gamma_l^{-})^{1/2} + 2(\gamma_l^{+}\gamma_s^{-})^{1/2} \quad (1)$$

Here subscripts l and s refer to liquid and solid, respectively. θ is the CA of liquid drop on solid surface and γ_l is the surface free energy of liquid probe. γ_s^{LW} and γ_l^{LW} are the apolar Lifshitz−van der Waals components of solid and liquid, respectively. γ_s^{+} and γ_l^{+} are the electron acceptor and γ_s^{-} and γ_l^{-} are the electron donor components of surface free energy of solid and liquid, respectively. For an apolar liquid, $\gamma_l^{+} = \gamma_l^{-} = 0$, that is, $\gamma_l = \gamma_l^{LW}$. Hence, eq 1 can be rewritten as follows

$$\gamma_s^{LW} = \gamma_l(1+\cos\theta)^2/4 \quad (2)$$

Consequently, the γ_s^{LW} of a solid surface can be calculated using the CA value of an apolar liquid probe. For a sample, this calculation was performed for apolar liqid (parffin oil); then, the γ_s^{LW} value was inferred. By using the known γ_s^{LW} value in eq 1, two unknown parameters (i.e., γ_s^{+} and γ_s^{-}) were fitted for two sets of water−formamide and water−glycerol. The results were averaged. The total surface energy of a solid (γ_s^{TOT}) and its relationship with dispersion (γ_s^{LW}) and acid−base (γ_s^{AB}) components are expressed as follows[21−23]

$$\gamma_s^{TOT} = \gamma_s^{LW} + \gamma_s^{AB} \quad (3)$$

$$\gamma_s^{AB} = 2(\gamma_s^{+}\gamma_s^{-})^{1/2} \quad (4)$$

The surface free energy components of the liquid probes are tabulated in Table 1.

Morphological and Compositional Characterization. *FTIR.* Fourier transform infrared (FTIR) spectrometry analysis was carried out in transmission mode with a Shimadzu 8400S instrument within the range of 500−4000 cm^{-1}.

SEM and AFM. Samples were coated with gold of ∼50 nm thickness using a SC7640 sputter coater (Quorum Technologies, Newhaven, U.K.) under vacuum (13.33 Pa), 1.2 kV, and 50 mA at (25 ± 1) °C. The surface morphology of coated samples was examined by scanning electron microscopy (SEM) with a Jeol JSM-5910 LV instrument at 20 kV.

An atomic force microscope (Park systems XE70 SPM controller LSF-100 HS) was used for recording the surface morphology of coated samples. The probes used in noncontact mode were a triangular Si_3N_4 cantilever with integrated tips (Olympus). The normal spring constant of the cantilever was 20 $N \cdot m^{-1}$, and the force between tip and sample was 0.87 nN.

Biocompatibility Investigations. *Sterilization.* All tested materials were sterilized by incubation in a solution of 1% penicillin−streptomycin for 2 h, followed by two washes in PBS prior to cell culture.

Osteoblasts Cell Culture. SaOs2 cells were cultured in DMEM supplemented with 10% FCS (Biochrom AG), 1% Glutamax, 50 $U \cdot mL^{-1}$ penicillin, and 50 $mg \cdot mL^{-1}$ streptomycin (Gibco). They were split 1:3 every 3 days and cultured in a 5% CO_2 humid atmosphere at 37 °C. For the biocompatibility experiments, 50 000 cells were seeded per sample in 24-well plates (TPP) and incubated for 72 h.

MTS Assay. We used the CellTiter 96 aqueous one solution cell proliferation assay kit from Promega to measure cell proliferation on L and OL samples, in conformity with manufacturer indications. We measured the optical density at 450 nm for 90 min after incubation with cells at 37 °C. Samples were tested in triplicate, and results were depicted as the average of the measured values. The absorbance values are proportional to the number of metabolically active cells on the surface of biomaterials.

Immunofluorescence Microscopy. The adhesion of cells to L and OL samples was investigated by immunofluorescence microscopy. The cells were fixed with 4% *p*-formaldehyde and permeabilized by 0.2% Triton-X-100 treatment. Alexa Fluor 594 conjugated Phalloidin (Invitrogen) was used to label actin filaments. The samples were mounted using Prolong antifade (Invitrogen) and visualized by a Nikon Eclipse E600W epifluorescence microscope. Pictures were taken using a Nikon digital light DS-SM camera and NIS-Elements BR Software.

Table 2. CA Data of Liquid Probes for L and OL Coatings

coating type	CA ± 2°			
	water	formamide	paraffin oil	glycerol
L	58	52	18	30
OL	59	44	17	33
L dropcast	23	45	19	38
OL dropcast	49	46	21	26

Table 3. Surface Free Energy and Its Components of L and OL Coatings ($mJ \cdot m^{-2}$)

coating type	γ_s^{LW}	γ_s^-	γ_s^+	γ_s^{AB}	γ_s^{TOT}
L	27.43	17.61	3.98	16.74	44.17
OL	27.72	14.19	5.15	17.10	44.82
L dropcast	27.34	61.63	1.33	18.07	45.41
OL dropcast	27.02	25.25	4.34	20.93	47.95

RESULTS AND DISCUSSION

CA Measurements. The surface free energy and its components (i.e., apolar Liftshitz−van der Waals, LW, and polar electron donor−electron acceptor interactions) of L- and OL-coated surfaces were determined by the sessile liquid drop in one-liquid method. The essential advantage of the CA technique over the spectroscopic ones (such as electron spectroscopy for chemical analysis (ESCA), Auger electron spectroscopy (AES),

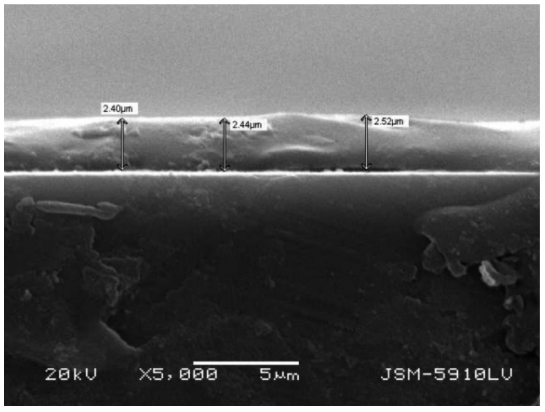

Figure 2. Typical XSEM of L thin films on glass obtained by MAPLE.

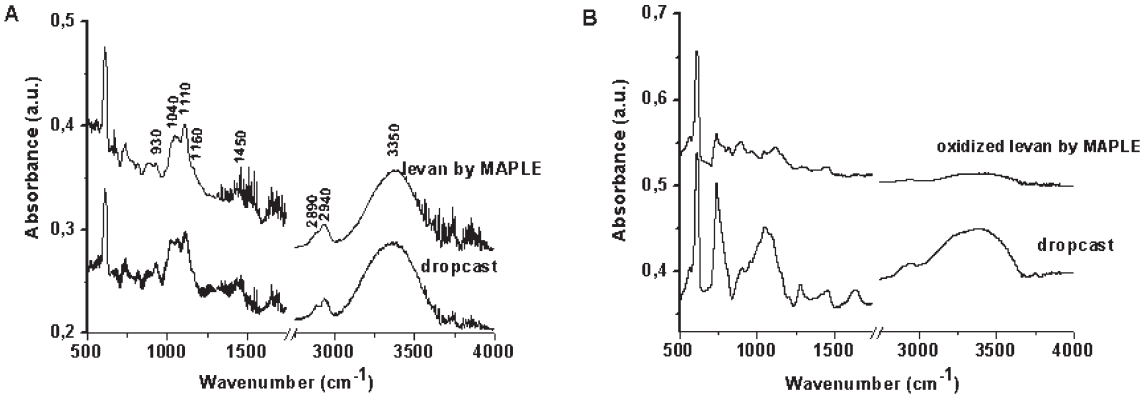

Figure 1. FTIR absorption spectra of (A) L dropcast and L and (B) OL dropcast and OL thin films deposited by MAPLE.

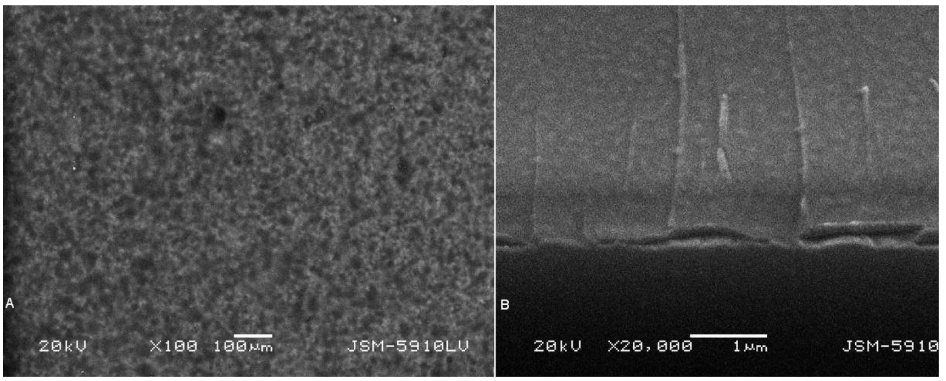

Figure 3. Surface SEM (A) and XSEM (B) of L thin films on glass obtained by MAPLE.

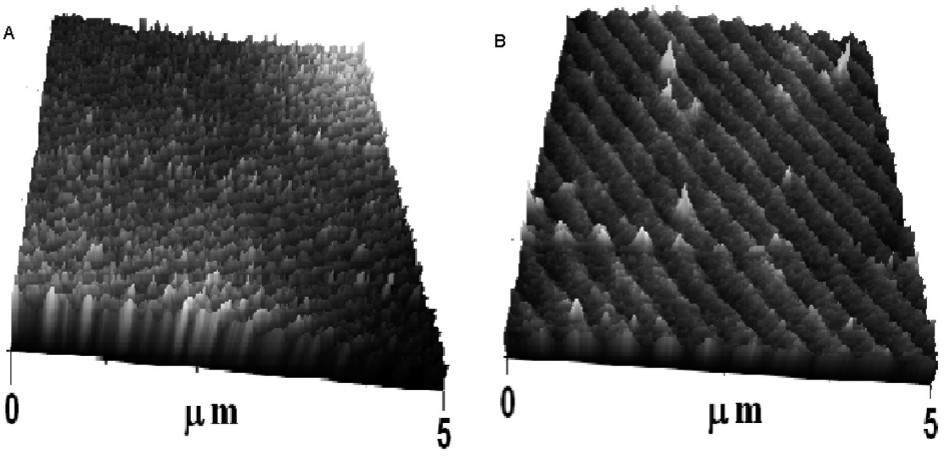

Figure 4. Typical AFM images of sample surfaces for (A) L and (B) OL coatings on Si.

and secondary ion mass spectroscopy (SIMS)) is that whereas these techniques require ultrahigh vacuum environment for analysis, it provides a quantitative evaluation of the surface dynamics of solid polymer under their application medium.

The surface dynamics of polymers is considerably different from that of rigid materials like ceramics and metals because of the high mobility of macromolecules at surface. Therefore, the composition of the polymer surfaces is generally different from that of the bulk and varies into the depth. Over the glass-transition temperature, because polymers undergo substantial segmental rotations and movements, their surface presents a dynamic nature. In nonpolar environments (e.g., air), the density of hydrophobic groups on the surface increases, whereas in a polar environment, the polar groups are oriented toward the surface, which becomes more energetic.[25−27]

CA data of liquid probes on L- and OL-coated surfaces and their calculated surface free energy components are collected in Tables 2 and 3, respectively.

Because of negligible deviations, values of γ_s^{LW} may be considered to be constant for all coating types (Table 3). However, their acid and base interactions are considerably different. On the basis of CA data, dropcast samples (L dropcast and OL dropcast) were found to have relatively higher basic character, which is an evidence of the surface enrichment with −O and −OH groups. Another important observation is that oxidized samples (OL and OL dropcast) showed higher hydrophilic acidic character than unmodified ones, most probably because of the more acidic aldehyde−hydrogen bonds of OL and OL dropcast formed after oxidation, which are oriented at surface.

FTIR Analysis. The congruent transfer by MAPLE of L and OL molecules from the frozen target to substrate was demonstrated by FTIR. To discriminate between the different compound spectra, we investigated separately L and OL dropcasts and films, respectively. Typical recorded absorption spectra are given in Figure 1A,B for the representative films, as compared with their corresponding dropcasts. Similar absorption bands of dropcast and MAPLE films were noticed for both L (Figure 1A) and OL (Figure 1 B) with peaks at 2890, 2940, and 3350 cm^{-1}, or 930, 1040, and 1110 cm^{-1}. All peaks are specific to levan either commercial or synthesized by *Halomonas* sp.,[6] confirming that the composition was preserved after dissolving the L and OL powders in DMSO (dropcast) or subsequent to MAPLE transfer.

Growth and Surface Morphology. Cross section SEM (XSEM) images (Figure 2) showed rather homogeneous and compact L and OL coatings with good adhesion to substrate. The surface looked quite smooth, and the variation in height across films was low (from 2.4 to 2.52 μm) over a relatively large area, which confirmed the uniformity of the layer. From film thickness, we could estimate a growth rate of 0.12 Å/laser pulse.

SEM observation of sample surfaces revealed an unusual 2D ordered array. A typical SEM image of L coating surface is shown in Figure 3 A. This controlled aggregation (assembling) at

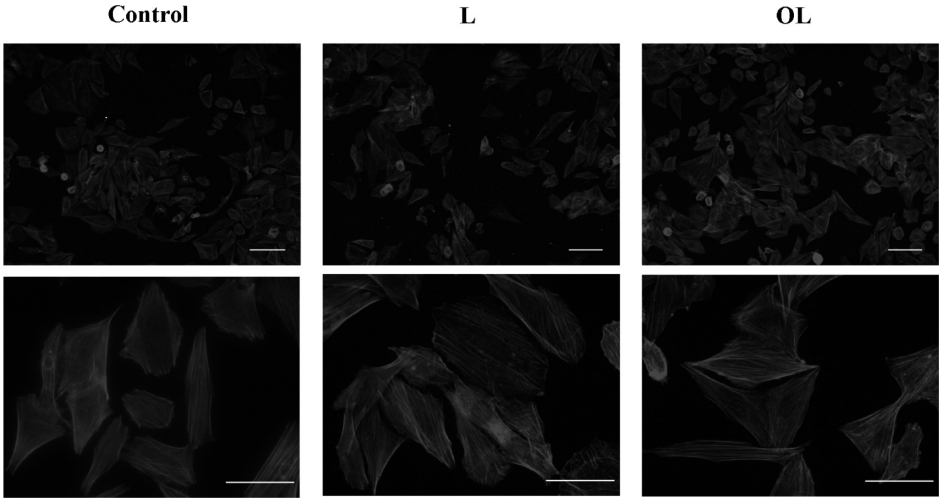

Figure 5. SaOs2 cells adhesion on control, L, and OL coatings on glass by immunofluorescence microscopy. Scale bars 100 (top) and 50 μm (bottom).

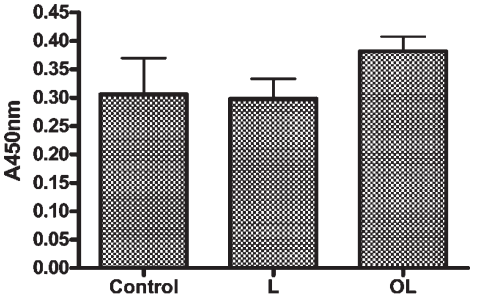

Figure 6. SaOs2 cells proliferation on L and OL coatings on glass by MTS assay.

Table 4. Roughness (rms, Ra, and Rz) Values for L and OL Coatings on Si Substrates

sample	rms (nm)	Ra (nm)	Rz (nm)
L coating on Si	0.972	0.762	4.158
OL coating on Si	1.203	0.962	4.818

surface was previously reported for nanohydroxyapatite (nHA) particles mixture with chitosan.[28] The nanostructured growth was proved by high-resolution XSEM studies (Figure 3 B). The surface features are confined in volume, confirming that the film assembling is starting from the bottom. The nanostructured assembling could be due to evaporation of the DMSO molecules that accompany L and OL species until the substrate. There, in contact with the heated substrate, the solvent molecules are quickly evaporated and evacuated. The flowing shallow layer is drying along a specific (evacuation) direction, and a large-scale orientation of the deposited phase is promoted. In literature, this phenomenon is described as "evaporation-induced self-assembly" (EISA).[29,30]

Typical 3D-AFM images of L and OL coatings are shown in Figure 4A,B. Surface assembling of L and OL was confirmed. Films morphology is similar in the two cases with a neat spatial orientation, probably because of the combined effect of evaporation-induced assembly with the specific linkages between the linear structures of polysaccharides. We noticed that the nanostructured assembling increases the specific surface area, which could boost surface properties.

As shown in Table 4, the roughness values (root mean square (rms), roughness arithmetic average (Ra) and the average height (Rz)) inferred from Figure 4 were found to be very small and rather similar in the case of MAPLE L and OL coatings.

Biocompatibility Studies. Adhesion of SaOs2 cells on L and OL coatings and control (borosilicate) glass material was investigated by fixing and then labeling the cells for actin filaments to examine cytoskeleton organization on coatings. Immunofluorescence microscopy images (Figure 5) show a similar coverage of the control and tested surfaces with bone cells. Moreover, no change in the filament organization pattern was seen when cells are grown on all coatings. Actin is uniformly spread throughout cell cytosol in parallel filaments sustaining cell shape and motility.

To assess the effect of L and OL coatings on cell viability and proliferation, we performed an MTS assay 72 h after seeding SaOs2 cells on their surface. The spectrofotometry data (Figure 6) showed that L and OL coatings have no detrimental function over bone cells. Osteoblasts proliferation was similar on L and control samples. As clearly visible from Figure 6, OL induces an increase in the ability of cells to divide and give rise to daughter cells, as proved by a higher absorbance value determined for this material. This result is in accordance with the expected outcome and is supported by CA measurements where hydrophilic surfaces were evidenced in the case of OL.

To conclude, all coatings presented a positive interaction with bone cells, which sustains cell adhesion and proliferation, key processes required for tissue integrity and function.

CONCLUSIONS

The transfer of pure levan and oxidized levan by MAPLE was successfully achieved without any addition of plasticizers or pigments. Use of MAPLE in this study enabled the deposition of this delicate biomaterial, which was unapproachable before by laser or other techniques. The coatings preserved the initial composition, as demonstrated by the IR absorption data. The samples presented a compact structure, good adhesion to substrate, and a uniform, homogeneous nanostructured surface. They exhibited high specific surface areas fully compatible with their potential use in biology or medicine. Cell viability and proliferation studies confirmed the biocompatible behavior of the synthesized nanostructures. The oxidized levan thin films induced an increase in cell proliferation as compared with the

simple levan coatings. This result is in good agreement with the contact angle data, which evidenced a higher hydrophilicity in case of oxidized levan samples, which was assigned to the acidic aldehyde−hydrogen bonds formed after oxidation.

AUTHOR INFORMATION

Corresponding Author
*E-mail: ion.mihailescu@inflpr.ro.

ACKNOWLEDGMENT

This work was supported by the bilateral contract 109T614 between Turkey and Romania. F.S., C.R., and I.N.M. acknowledge with thanks the partial support of this work by *UEFISCSU, IDEI 511/2009* contract.

REFERENCES

(1) Kazak, H.; Öner, E. T.; Dekker, R. F. H. In *Handbook of Carbohydrate Polymers: Development, Properties and Applications*; Ito, R., Matsuo, Y., Eds.; Nova Science Publishers: New York, 2009; p 605.
(2) Nicolaus, B.; Kambourova, M.; Toksoy Öner, E. *Environ. Technol.* **2010**, *31*, 1145–1158.
(3) Poli, A.; Kazak, H.; Gürleyendağ, B.; Tommonaro, G.; Pieretti, G.; Toksoy Öner, E.; Nicolaus, B. *Carbohydr. Polym.* **2009**, *78*, 651–657.
(4) Kang, S. A.; Jang, K. H.; Seo, J. W.; Kim, K. H.; Kim, Y. H.; Rairakhwada, D.; Seo, M.; Lee, J. O.; Ha, S. D.; Kim, C. H.; Rhee, S. K. In *Microbial Production of Biopolymers and Polymer Precursors*; Rehm, B. H. A., Eds.; Caister Academic Press: Wymondham, U.K., 2009; p 145.
(5) Sezer, A. D.; Kazak, H.; Toksoy Oner, E.; Akbuğa, J. *Carbohydr. Polym.* **2011**, *84*, 358–363.
(6) Küçükaşık, F.; Kazak, H.; Güney, D.; Finore, I.; Poli, A.; Yenigün, O.; Nicolaus, B.; Toksoy Öner, E. *Appl. Microbiol. Biotechnol.* **2011**, *89*, 1729–1740.
(7) Simon, J.; Muller, H. P.; Koch, R.; Muller, V. *Polym. Degrad. Stab.* **1998**, *59*, 107–115.
(8) Guan, J. J.; Hanna, M. A. *Bioresour. Technol.* **2006**, *97*, 1716–1726.
(9) Barone, J. R.; Medynets, M. *Carbohyd. Polym.* **2007**, *69*, 554–556.
(10) Kim, S. S.; Hyun, J. C. In *Handbook of Solvents*; Wypych, G., Ed.; William Andrew Publishing: Norwich, NY, 2001; p 410.
(11) Pique, A. In *Pulsed Laser Deposition of Thin Films: Applications-Led Growth of Functional Materials*; Eason, R., Ed.; John Wiley & Sons: Hoboken NJ, 2008; p 63.
(12) Zergioti, I.; Karaiskou, A.; Papazoglou, D. G.; Fotakis, C.; Kapsetaki, M.; Kafetzopoulos, D. *Appl. Phys. Lett.* **2005**, *86*, 163902/1–163902/3.
(13) Patz, T. M.; Doraiswamy, A.; Narayan, R. J.; He, W.; Zhong, Y.; Bellamkonda, R.; Modi, R.; Chrisey, D. B. *J. Biomed. Mater. Res., Part B* **2006**, *78B*, 124–130.
(14) Klini, A.; Manousaki, A.; Anglos, D.; Fotakis, C. *J. Appl. Phys.* **2005**, *98*, 123301/1–123301/8.
(15) Sima, F.; Axente, E.; Ristoscu, C.; Mihailescu, I. N.; Kononenko, T. V.; Nagovitsin, I. A.; Chudinova, G.; Konov, V. I.; Socol, M.; Enculescu, I.; Sima, L. E.; Petrescu, S. M. *J. Biomed. Mater. Res.* **2011**, *96A*, 384–394.
(16) Piqué, A.; Auyeung, R. C. Y.; Stepnowski, J. L.; Weir, D. W.; Arnold, C. B.; McGill, R. A.; Chrisey, D. B. *Surf. Coat. Technol.* **2003**, *163−164*, 293–299.
(17) Cristescu, R.; Doraiswamy, A.; Patz, T.; Socol, G.; Grigorescu, S.; Axente, E.; Sima, F.; Narayan, R. J.; Mihaiescu, D.; Moldovan, A.; Stamatin, I.; Mihailescu, I. N.; Chisholm, B.; Chrisey, D. B. *Appl. Surf. Sci.* **2007**, *253*, 7702–7706.
(18) Floroian, L.; Sima, F.; Florescu, M.; Badea, M.; Popescu, A. C.; Serban, N.; Mihailescu, I. N. *J. Electroanal. Chem.* **2010**, *648*, 111–118.
(19) Vina, I.; Karsakevich, A.; Bekers, M. *J. Mol. Catal. B: Enzym.* **2001**, *11*, 551–558.
(20) Dogan, M.; Eroglu, M. S.; Erbil, H. Y. *J. Appl. Polym. Sci.* **1999**, *74*, 2848–2455.
(21) Good, R. J. In *Contact Angle Wettability and Adhesion*; Mittal, K. L., Ed.; VSP Press: Utrecht, The Netherlands, 1993; p 3.
(22) Van Oss, C. J. *Interfacial Forces in Aqueous Media*; Marcel Dekker: New York, 1994.
(23) Van Oss, C. J.; Chaudhury, M. K.; Good, R. J. *Chem. Rev.* **1998**, *88*, 927–941.
(24) Van Oss, C. J.; Good, R. J. *Langmuir* **1992**, *8*, 2877–2879.
(25) Chatelier, R. C.; Xie, X.; Gengenbach, T. R.; Griesser, H. J. *Langmuir* **1995**, *11*, 2576–2584.
(26) Eroglu, M. S. *J. Appl. Polym. Sci.* **2006**, *101*, 3343–3347.
(27) Erbil, H. Y.; Yasar, B.; Suzer, S.; Baysal, B. M. *Langmiur* **1997**, *13*, 5484–5493.
(28) Kumar, R.; Prakash, K. H.; Cheang, P.; Gower, L.; Khor, K. A. *J. R. Soc., Interface* **2008**, *5*, 427–439.
(29) Jeffrey Brinker, C.; Lu, Y.; Sellinger, A.; Fan, H. *Adv. Mater.* **1999**, *11*, 579–585.
(30) Brezesinski, T.; Groenewolt, M.; Gibaud, A.; Pinna, N.; Antonietti, M.; Smarsly, B. M. *Adv. Mater.* **2006**, *18*, 2260–2263.